

X-ray diffraction study of plastic relaxation in Ge-rich SiGe virtual substrates

Viktor S. Kopp* and Vladimir M. Kaganer

Paul Drude Institut für Festkörperelektronik, Hausvogteiplatz 5-7, D-10117 Berlin, Germany

Giovanni Capellini and Monica De Seta

Dipartimento di Fisica "E. Amaldi," Università di Roma Tre, via Vasca Navale 84, 00146 Rome, Italy

Peter Zaumseil

IHP, Im Technologiepark 25, 15236 Frankfurt (Oder), Germany

(Received 27 April 2012; published 19 June 2012)

We report on the experimental and theoretical investigation of the relaxation in Ge-rich SiGe/Ge/Si heterostructures. The experimental x-ray diffraction data are interpreted with the help of a model including both edge and 60° misfit dislocations in the calculated x-ray scattering intensity. Our results show that highly positionally correlated edge dislocations dominate in the relaxation of the compressive strain at the Ge/Si interface, while a smaller tensile strain at the SiGe/Ge interfaces released by uncorrelated/little correlated 60° dislocations.

DOI: [10.1103/PhysRevB.85.245311](https://doi.org/10.1103/PhysRevB.85.245311)

PACS number(s): 61.05.cp, 61.72.-y, 61.72.uf

I. INTRODUCTION

Strained Ge is a promising material both for electronic¹ and optoelectronic applications² and its monolithic integration in Si microelectronics is highly desirable. The amount of strain impacting the electronic and optical properties can be tuned upon deposition of the Ge layer on suitably designed SiGe virtual substrates (VS). Among many other VS, the use of reverse graded SiGe VS (RGVS) has recently been proposed.^{3,4} In such structures a thick, relaxed Ge heteroepitaxial layer is first deposited on a Si(001) substrate. Subsequently, the desired in-plane lattice parameter for the Ge epilayer growth is achieved upon decreasing the Ge content x in a sequence of $\text{Si}_{1-x}\text{Ge}_x$ layers in which the strain is relaxed via the insertion of misfit dislocations. It is therefore of paramount importance to understand the plastic relaxation mechanisms of the virtual substrate governing the dislocation formation and evolution.

In epitaxial heterostructures comprising diamond-lattice semiconductors, the lattice mismatch is plastically relaxed when the deposited epilayer reaches a critical thickness. In case of compressive misfit f , i.e., when the epilayer has an in-plane lattice parameter larger than that of the substrate, two different behaviors are usually observed for large ($f > 2\%$) and small misfits ($f < 2\%$), respectively (see reviews in Refs. 5–7). In the former case, the strain is released mostly by 90° (edge, Lomer type) dislocations having their Burger vectors entirely contained heterointerface plane. These 90° dislocations can glide along the heterointerface. This mobility enables the almost periodic arrangements of the dislocation lines aligned along the $[110]$ -equivalent directions, resulting in a further reduction of elastic energy.

On the contrary, small misfits are relaxed via 60° misfit dislocations that are either nucleated at the film free surface or as a result of the motion of threading dislocations already present in the film. The glide along $\{111\}$ planes allow them to reach the heterointerface and form misfit segments, always terminated by threading arms.

In the less studied tensile heterostructures, particularly, the ones forming the RGVS, a clear picture of the relaxation

mechanisms is still missing. It has been recently proposed³ that, at least for small f , little correlated 60° misfit dislocations are the main contributors to the strain release.

X-ray diffractometry is routinely employed in the studies of relaxed epitaxial films. Its primary use is to obtain precise values of lattice parameters from diffraction peak positions. By comparing a symmetric and an asymmetric reflection, one can separately determine the mismatch (i.e., the Ge concentration) and the degree of relaxation.⁸ If the dislocation type is known, the dislocation density can be calculated from the degree of relaxation.

To determine the dislocation types and their correlations from the x-ray diffraction peaks, the analysis of the whole diffraction pattern is needed. The scattering from crystals with dislocations is described by the kinematical diffraction theory, and general formulas for the x-ray intensity can be readily formulated.^{9,10} However, they involve statistical average over dislocation ensemble. If statistical properties of dislocation distribution are known, the scattering intensity from misfit dislocations can be calculated by Monte Carlo methods.¹¹ A notable simplification is reached in the case of large dislocation densities, when the film thickness is large compared to the mean distance between dislocations. In this case, the positional correlations between dislocations can be easily included, if the correlation length is also smaller than the film thickness.^{10,12}

The x-ray scattering theory has been also extended to epitaxial films consisting of layers with different composition and relaxation degree, and to graded layers.^{13–17} These works use additional approximations that simplify the scattering intensity calculation. Particularly, they assume that dislocations of only one type (the 60° dislocations) are present in the film and that the positional correlations are absent.

In this study, we compare x-ray scattering calculations and XRD measurements for heterostructures containing several types of dislocations, with different correlation degrees between them. We show that dislocation types, densities, and correlations can be obtained from the x-ray reciprocal space maps. We find that the large misfit between Si substrate and Ge buffer layer is mostly released by correlated 90° dislocations,

while the smaller tensile misfit between $\text{Si}_{1-x}\text{Ge}_x$ layers and Ge buffer is released mainly by 60° dislocations that are observed to be only little correlated.

II. EXPERIMENTAL

The two samples investigated in this study were grown by means of an ultrahigh vacuum chemical vapor deposition technique (UHV-CVD) using ultrahigh pure silane and germane on Si(001) substrates. After an *ex situ* wet cleaning, the substrates are loaded in a fast entry load lock and annealed at 1100°C in H_2 in order to remove contaminants from the surface. Subsequently, a 500-nm thick silicon layer is deposited at 800°C in order to improve the morphological and structural quality of the substrate. In order to obtain the relaxed Ge/Si system forming the first part of our RGVS, we have used a two-temperature UHV-CVD. The first deposition step occurs at a temperature 330°C . At such low temperature, the adsorption of GeH_4 molecules and the subsequent incorporation of Ge atoms is limited by the desorption of the H atoms. This kinetic effect hinders the Stranski-Krastanov growth expected for the Ge-Si system¹⁸ and favors the plastic relaxation of the Ge heteroepitaxial layer via the insertion of misfit dislocations. After the complete relaxation is achieved, the growth temperature can be increased to accelerate the growth and to improve the structural quality of the deposited crystal. Details of the complex temperature profile used to obtain the rest of the 1000-nm thick Ge layer can be found in Ref. 19.

On top of the Ge layer at 500°C , we deposited a 700-nm thick constant composition $\text{Si}_{0.15}\text{Ge}_{0.85}$ layer (sample 1) or a step graded reverse $\text{Si}_{1-x}\text{Ge}_x$ multilayer whose composition decreases from $x = 1.00$ down to $x = 0.83$ in 700 nm (sample 2). Notice that the last 100 nm of the graded layer have a silicon contents slightly higher than the subsequent thick cap layer in order to reduce the dislocation density at the topmost heterointerface, thus improving the expected crystal quality of the virtual substrate. The process pressure of this part of the RGVS was 4 mTorr, leading to a growth rate ~ 20 nm/min. Both samples were completed with a 900-nm thick $\text{Si}_{0.15}\text{Ge}_{0.85}$ cap layer grown at 1 mTorr (~ 5 nm/min). A detailed analysis of RGVSs is beyond the scope of this paper and going to be presented elsewhere.²⁰ A SmartLab diffractometer from Rigaku equipped with a 9 kW rotating anode Cu source in line focus geometry was used with $\text{Ge}(400)\times 2$ crystal collimator and $\text{Ge}(220)\times 2$ crystal analyzer to carry out the x-ray measurements.

III. THEORY

A. X-ray intensity from relaxed epitaxial films

Our aim is to calculate the x-ray scattering intensity from a relaxed heteroepitaxial multilayer film with dislocations, possibly of different types and with different positional correlations, located at a number of different interfaces, as shown schematically in Fig. 1. In this section, we formulate the general expressions for the scattering intensity from a relaxed film¹⁰ in a way that allows a direct generalization to the case of several layers.

Let us begin with the general expressions for the scattering intensity from a distorted crystal.⁹ Crystal lattice defects are

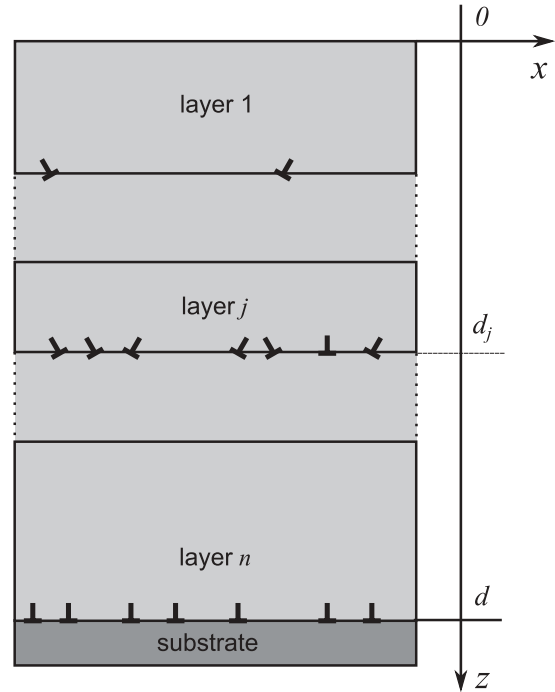


FIG. 1. Geometry of the network of dislocations in a stepped heteroepitaxial system.

atoms displaced from their ideal positions in the periodic lattice. The displacements can vary on distances much larger than the unit cell size, so that each unit cell is displaced as a whole. The position of a unit cell in a crystal with lattice defects is given by the sum $\mathbf{R}_s + \mathbf{U}(\mathbf{R}_s)$ of the position \mathbf{R}_s of this unit cell in a reference periodic lattice and its displacement $\mathbf{U}(\mathbf{R}_s)$. The index s runs over all the lattice cells. We consider here strongly distorted crystals, with the x-ray scattering intensity concentrated in the vicinity of the reciprocal lattice points. Then the intensity $I(\mathbf{q})$ depends only on the deviation $\mathbf{q} = \mathbf{Q} - \mathbf{Q}_0$ of the scattering vector \mathbf{Q} from the nearest reciprocal-lattice vector \mathbf{Q}_0 of the reference lattice. In the kinematic approximation, the expression for the x-ray scattering intensity can be written as a Fourier integral:⁹

$$I(\mathbf{q}) = \iint d\mathbf{R}_s d\mathbf{R}_{s'} e^{i\mathbf{q}\cdot(\mathbf{R}_s - \mathbf{R}_{s'})} G(\mathbf{R}_s, \mathbf{R}_{s'}) \quad (1)$$

of the correlation function $G(\mathbf{R}_s, \mathbf{R}_{s'})$ defined as

$$G(\mathbf{R}_s, \mathbf{R}_{s'}) = \langle \exp\{i\mathbf{Q} \cdot [\mathbf{U}(\mathbf{R}_s) - \mathbf{U}(\mathbf{R}_{s'})]\} \rangle. \quad (2)$$

The unit cell structure factor for the actual reflection gives a constant factor to Eq. (1) that is omitted here. The integration in Eq. (1) is carried out over the sample volume. The angular brackets in Eq. (2) stand for statistical average over the random positions of lattice defects.

For an epitaxial film, the substrate can be taken as the reference lattice. The displacement $\mathbf{U}(\mathbf{R})$ consists of two terms: (i) the displacement \mathbf{U}^c of the pseudomorphic film due to the difference in lattice parameters with the substrate and (ii) the displacement \mathbf{U}^d caused by the dislocations at a heterointerface. Only \mathbf{U}^d is the argument of the statistical average over the random positions of the dislocations, while

\mathbf{U}^c is a deterministic function (an explicit expression is given below) and can be taken out of the average (2).

The triple-crystal x-ray diffractometry provides high collimation of the incoming and the outgoing beams in the scattering plane, while in the direction normal to this plane a broad angular acceptance is allowed (the vertical divergence of the beam in a standard diffractometer setup). As a result, the scattering intensity (1) is integrated in the triple-crystal measurements by the wave vector component q_y normal to the scattering plane. Integration over q_y in Eq. (1) gives rise to a delta-function $\delta(R_{s_y} - R_{s'_y})$. As a result, two points \mathbf{R}_s and $\mathbf{R}_{s'}$ in Eq. (2) lie in one same plane $y = \text{const}$, where the integration in Eq. (1) is carried out. The integration over the film of thickness d (possibly comprising several layers, as in Fig. 1) can be finally written as¹⁰

$$I(q_x, q_z) = \iint_0^d dz_1 dz_2 \int_{-\infty}^{\infty} dx e^{iq_x x + iq_z(z_1 - z_2)} \times e^{i\mathbf{Q} \cdot [U_z^c(z_1) - U_z^c(z_2)]} G^d(x, z_1, z_2), \quad (3)$$

where the correlation function for dislocations is

$$G^d(x, z_1, z_2) = \langle e^{i\mathbf{Q} \cdot [\mathbf{U}^d(\mathbf{R}_1) - \mathbf{U}^d(\mathbf{R}_2)]} \rangle. \quad (4)$$

Here, we take into account that the correlations between two points (x_1, z_1) and (x_2, z_2) depend on the distance between these points in the plane of interface $x = x_1 - x_2$, as a result of the translational symmetry. However, the depths z_1 and z_2 enter the equations separately, because of a final film thickness.

The displacement in a pseudomorphic film \mathbf{U}^c has the only nonzero component in the direction of surface normal, $U_z^c(z)$, since the lateral spacing of a pseudomorphic film is kept equal to that of the substrate. The requirement of the absence of the normal stress at the surface gives

$$\frac{dU_z^c}{dz} = \frac{1 + \nu}{1 - \nu} f^0(z), \quad (5)$$

where $f^0(z)$ is the misfit between the layer and the substrate lattices at a distance z from the surface, ν is the Poisson ratio. For a film consisting of layers with constant misfit, considered in the present paper, U_z^c is a piece-linear function of z . We restrict ourselves to the isotropic approximation, since both Si and Ge possess rather little anisotropy, with the anisotropy ratio $A = 2c_{44}/(c_{11} - c_{12})$ equal to 1.56 and 1.66, respectively. Such anisotropy has a minor effect on the x-ray diffraction images of dislocations.²¹ We use the same value of the Poisson ratio $\nu = 0.275$ for both materials.

The dislocation displacement $\mathbf{U}^d(\mathbf{R})$ at a point \mathbf{R} in the film is caused by all dislocations at all interfaces in the film. Owing to linearity, it is just the sum of displacements due to individual dislocations, $\mathbf{U}^d(\mathbf{R}) = \sum_{j,p,t} \mathbf{u}_j^{(p)}(\mathbf{R} - \mathbf{R}_t)$, where p denotes different types of dislocations (i.e., different Burgers vectors and dislocation line directions), j stands for summation over different interfaces, \mathbf{R}_t are dislocation positions, and $\mathbf{u}(\mathbf{R})$ is the displacement field of a dislocation. For misfit dislocations lying parallel to the surface, $\mathbf{u}(\mathbf{R})$ can be represented as a sum of three terms, displacement due to a dislocation in the infinite medium, the image dislocation, and an additional surface relaxation term. Explicit expressions for all components of the Burgers vector are given in Appendix B of Ref. 10.

Evaluation of x-ray intensity (3) requires calculation of correlation function $G^d(x, z_1, z_2)$ for a given statistical distribution of dislocations. The statistical average can be done numerically by means of Monte Carlo methods.¹¹ However, if the dislocation density is sufficiently large and the correlations between dislocation positions can be neglected, the calculation can be drastically simplified.^{9,10} In this case, only the correlations between close points are of interest and the differences of displacements $\mathbf{Q} \cdot [\mathbf{U}^d(\mathbf{R}_1) - \mathbf{U}^d(\mathbf{R}_2)]$ can be replaced by distortions $\partial[\mathbf{Q} \cdot \mathbf{U}^d(\mathbf{R})]/\partial \mathbf{R}$. The correlation function can be represented as $G^d(x, z_1, z_2) = \exp[-T(x, z_1, z_2)]$, and $T(x, z_1, z_2)$ is expanded in power series of the distance $\mathbf{R}_1 - \mathbf{R}_2$. The linear term in the expansion is imaginary and the quadratic term is real:

$$\text{Im } T(x, z, \zeta) = q_x^d(z)x + q_z^d(z)\zeta, \quad (6)$$

$$\text{Re } T(x, z, \zeta) = w_{xx}(z)x^2 + 2w_{xz}(z)x\zeta + w_{zz}(z)\zeta^2, \quad (7)$$

where x and $\zeta = z_1 - z_2$ are the components of the vector $\mathbf{R} = \mathbf{R}_1 - \mathbf{R}_2$. The components of the vector $\mathbf{q}^d(z)$ in Eq. (6) are calculated as

$$q_x^d(z) = - \sum_{j,p} \rho_j^{(p)} \int_{-\infty}^{\infty} dx \frac{\partial \mathbf{Q} \cdot \mathbf{u}_j^{(p)}}{\partial x}, \quad (8)$$

$$q_z^d(z) = - \sum_{j,p} \rho_j^{(p)} \int_{-\infty}^{\infty} dx \frac{\partial \mathbf{Q} \cdot \mathbf{u}_j^{(p)}}{\partial z}, \quad (9)$$

and the components of the 2×2 symmetrical matrix $\hat{w}(z)$ in Eq. (7) are

$$w_{mn}(z) = \sum_{j,p} \frac{\rho_j^{(p)}}{2} \int_{-\infty}^{\infty} dx \frac{\partial \mathbf{Q} \cdot \mathbf{u}_j^{(p)}}{\partial x_m} \frac{\partial \mathbf{Q} \cdot \mathbf{u}_j^{(p)}}{\partial x_n}. \quad (10)$$

Here, $\rho_j^{(p)}$ is the linear density of the dislocations of type p at the j th interface, x_m and x_n stand for x or z .

The integration over x and ζ is performed analytically, and the diffracted intensity (3) is represented as

$$I(q_x, q_z) = \pi \int_0^d \frac{dz}{\sqrt{\det[\hat{w}(z)]}} \times \exp \left[-\frac{1}{4} w_{mn}^{-1}(z) (\mathbf{q} - \mathbf{q}^0(z))_m (\mathbf{q} - \mathbf{q}^0(z))_n \right], \quad (11)$$

where $\mathbf{q}^0 = \mathbf{q}^d + \mathbf{q}^c$ contains both the dislocation (8), (9), and composition related

$$q_z^c = \frac{1 + \nu}{1 - \nu} Q_z f^0(z) \quad (12)$$

shift of the peak position for each layer in the film.

B. X-ray intensity from a multilayer film

The general expression for the scattering intensity (11) and the expressions for the vector \mathbf{q}^0 and the matrix \hat{w} are formally the same of those holding for the x-ray intensity scattered from a system comprising a single epitaxial layer on a substrate, with the dislocation network located at the heterointerface.¹⁰ In case of several stacked heteroepitaxial layers with dislocations at heterointerfaces, the calculation of \mathbf{q}^0 and \hat{w} is more

complicated. As a matter of fact, the contribution from each interface to \mathbf{q}^0 and \hat{w} should be calculated separately at points above and below the interface. The explicit expressions are derived below.

The substitution of explicit formulas for dislocation displacements into Eqs. (8)–(10) enables the analytical calculation of integrals. The wave vectors defining the peak position are

$$\begin{aligned} q_x^0(z) &= -Q_x \sum_{j,p} b_{jx}^{(p)} \rho_j^{(p)} H(d_j - z), \\ q_z^0(z) &= -\frac{\nu}{1-\nu} Q_z \sum_{j,p} b_{jx}^{(p)} \rho_j^{(p)} H(d_j - z) + q_{jz}^c, \end{aligned} \quad (13)$$

where $b_{jx}^{(p)}$ is the mismatch-releasing component of the Burgers vector of dislocations of type p at the j th interface. The distance of the interface from the surface $z = 0$ is d_j , see Fig. 1. $H(x - x')$ is the step-like Heaviside function. Equation (13) shows that the peak position of a j th layer is affected only

by the dislocations laying at and under the j th interface, since for $z > d$ the integrals $\int_{-\infty}^{\infty} dx \partial(\mathbf{Q} \cdot \mathbf{u})/\partial x = 0$ and $\int_{-\infty}^{\infty} dx \partial(\mathbf{Q} \cdot \mathbf{u})/\partial z = 0$.

When calculating the elements of the matrix \hat{w} , it is needed to take into account that the dislocations at the interface $z = d_j$ contribute to this matrix for the layers both above and below the interface, so that the matrix elements can be represented as

$$w_{mn}(z) = \sum_{j,p} [w_{mn}^{(j,p)}(z)H(d_j - z) + \tilde{w}_{mn}^{(j,p)}(z)H(z - d_j)] \quad (14)$$

with different expressions for $w_{mn}^{(j,p)}(z)$ and $\tilde{w}_{mn}^{(j,p)}(z)$. They can be evaluated analytically by substituting the dislocation displacements given in Appendix B of Ref. 10 into Eq. (10). The final expressions are bulky. In order to demonstrate their structure, we present here one of the integrals for dislocations with Burgers vector $\mathbf{b}(b_x, 0, 0)$: for $z < d$,

$$\begin{aligned} \int_{-\infty}^{\infty} \frac{\partial u_x}{\partial x} \frac{\partial u_z}{\partial z} dx &= \frac{b_x^2}{\pi} \left[-\frac{z^2 \alpha^2}{4d^3} - \frac{3z^4 \alpha^2}{4(d+z)^5} + \frac{3z^3 \alpha^2}{2(d+z)^4} - \frac{\alpha^2}{8d} + \frac{z\alpha^2}{8d^2} \right. \\ &\quad \left. + \frac{2-4\alpha+\alpha^2}{16(d-z)} + \frac{2-4\alpha+\alpha^2}{16(d+z)} + \frac{-2z+4z\alpha-z\alpha^2}{8(d+z)^2} + \frac{2z^2-4z^2\alpha-5z^2\alpha^2}{8(d+z)^3} \right], \end{aligned}$$

while for $z > d$,

$$\begin{aligned} \int_{-\infty}^{\infty} dx \frac{\partial u_x}{\partial x} \frac{\partial u_z}{\partial z} &= \frac{b_x^2}{\pi} \left[\frac{d^2 \alpha^2}{4z^3} - \frac{3d^4 \alpha^2}{4(d+z)^5} + \frac{3d^3 \alpha^2}{2(d+z)^4} + \frac{-2+4\alpha-\alpha^2}{8z} + \frac{2d-4d\alpha+d\alpha^2}{8z^2} \right. \\ &\quad \left. + \frac{-2+4\alpha-\alpha^2}{16(d-z)} + \frac{2-4\alpha+\alpha^2}{16(d+z)} + \frac{-2d+4d\alpha-d\alpha^2}{8(d+z)^2} + \frac{2d^2-4d^2\alpha-5d^2\alpha^2}{8(d+z)^3} \right]. \end{aligned}$$

Here, it is denoted $\alpha = 1/[2(1-\nu)]$. Then, integral for x-ray intensity (11) remains to be calculated numerically.

C. Positional correlations of dislocations

The formulas above are derived assuming that dislocation positions at a heterointerface are random and independent. One can expect that the dislocations are positionally correlated, to reduce the elastic energy. Although the elastic energy has a minimum for periodic dislocations, this arrangement can not be achieved in many cases. Particularly, the 60° dislocations have inclined glide planes that allow them to penetrate into the film but do not allow to glide along the interface. On the other hand, the edge Lomer dislocations can glide along the interface and therefore can reach a state much closer to a periodic arrangement.

The account of correlations in a general case is fairly complicated, based on the cumulant expansion.⁹ When the dislocation density is large (practically, it is enough if the mean distance between dislocations is smaller than the film thickness), the x-ray intensity from correlated dislocations can be calculated in quadratures.¹¹ Further simplification is obtained when the correlation length of the positional correlations is small compared to the film thickness. It was initially suggested¹⁰ and recently argued in details,¹² that in

this case, the effect of correlations reduce, for each type of dislocations, to a constant factor $g^{(p)}$ that vary from 0 to 1. The limiting value $g^{(p)} = 1$ corresponds to uncorrelated dislocations, while the opposite limit $g^{(p)} \rightarrow 0$ corresponds to periodic dislocations. In this approximation, the account of correlations simply consists in replacement of all matrix elements $w_{mn}^{(j,p)}$ and $\tilde{w}_{mn}^{(j,p)}$ in Eq. (14) with $g^{(p)}w_{mn}^{(j,p)}$ and $g^{(p)}\tilde{w}_{mn}^{(j,p)}$. Presence of correlations does not affect the imaginary part of the correlation function $\text{Im} T(x, z, \zeta)$. Hence the positions of diffraction peaks do not depend on the dislocation correlations, while the widths of the diffraction peaks decrease with the increasing correlations.

D. Example: two-layer film with different types of dislocations

Before proceeding to analysis of the experimental data, let us calculate x-ray diffraction peaks for a model epitaxial system consisting of two layers with different types of dislocations at two interfaces. The model system is sketched in Fig. 2(a). The parameters are chosen to be close to the experimental systems considered in the next section. The top layer (layer 1) has a thickness of $1.6 \mu\text{m}$, while the bottom layer is $1.0\text{-}\mu\text{m}$ thick. The interface 1 between the layers is populated by uncorrelated 60° dislocations with density $\rho_1 = (36.2 \text{ nm})^{-1}$. The interface 2 between the layer 2 and the substrate

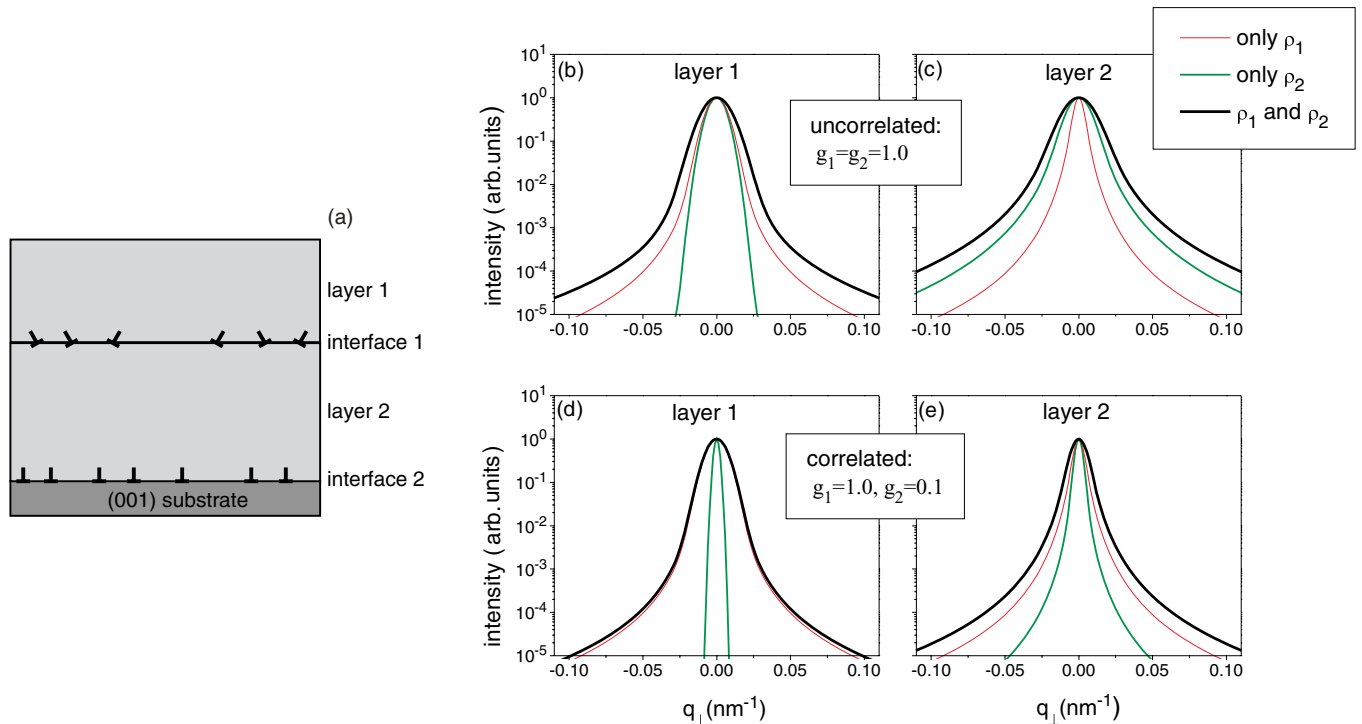


FIG. 2. (Color online) (a) A model epitaxial film consisting of two layers with 60° dislocations at the top interface and 90° at the bottom interface. (b)–(e) Transverse scans through symmetrical (004) reflection: (b) and (c) uncorrelated dislocations on both interfaces, (d) and (e) uncorrelated dislocations at the top interface and correlated dislocations at the bottom interface.

contains 90° dislocations having density $\rho_2 = (9.1 \text{ nm})^{-1}$, either uncorrelated ($g_2 = 1$) or correlated ($g_2 = 0.1$).

In Figs. 2(b)–2(e), the transverse scans through symmetric (004) reflection are shown. The peaks from both layers are presented. Figure 2(b) compares the peaks of layer 1 obtained for uncorrelated dislocations at both interfaces (black line), only at the interface 1 (red line), and only at the interface 2 (green line). Dislocations at either top or bottom interface cause broadening of the peak, and a collective effect of both dislocation networks is larger than any of them alone. Similarly, Fig. 2(c) shows that the dislocations at both interfaces influence the peak of layer 2.

In Figs. 2(d) and 2(e) the dislocations at the lower interface are taken correlated, $g_2 = 0.1$. They cause very little effect on the peak 1 but provide some broadening of the peak 2. Still, the peak 2 remains narrower than in the case of uncorrelated dislocations. The diffraction peaks for the model two-layer system in Fig. 2 show that calculation of any peak needs to include contributions from dislocations at all interfaces in the film. Positional correlations of dislocations reduce the contribution of the respective interface. Particularly, strong correlations between dislocations at some interface result in very small contribution of this interface to diffraction peaks of the other layers.

IV. RESULTS

A. Calculation method and parameters

The reciprocal space maps (RSMs) near symmetric (004) and asymmetric ($\bar{2}24$) reflections have been used to determine the dislocation types, densities, and correlations. The

diffracted intensity has been calculated with the equations given above, allowing both edge and 60° dislocations at each interface. Dislocations in each set can be positionally correlated.

We assume that the dislocations are oriented along the [110] and $[1\bar{1}0]$ directions with equal densities and distributions. Burgers vectors of the dislocations with the line direction perpendicular to the scattering plane are $\mathbf{b} = a(1/\sqrt{2}, 0, 0)$ for 90° (edge) and $\mathbf{b} = a/2(1/\sqrt{2}, \pm 1/\sqrt{2}, \pm 1)$ for 60° dislocations. Here, a is the substrate lattice spacing. All dislocations possess the same sign of the b_x component of the Burgers vector, that releases the misfit. The signs of other components (screw and tilt components b_y and b_z) are realized with equal probabilities and without correlations.

The parameters to be determined for each layer are the Ge concentration of the $\text{Si}_{1-x}\text{Ge}_x$ alloy, and densities and correlations for dislocations of two possible types. The RSMs contain enough information to obtain all these unknowns. First, the positions of the diffraction peaks from a given layer in a symmetric and an asymmetric RSMs allow to determine the misfit and strain. The actual in-plane strain of a layer is defined with respect to its cubic state

$$\epsilon = (a_x - a_x^0)/a_x^0, \quad (15)$$

where a_x and a_x^0 are the measured in-plane and fully relaxed (cubic) lattice parameters of the evaluated layer, respectively. The Ge content in $\text{Si}_{1-x}\text{Ge}_x$ alloys is calculated using the quadratic dependence of the misfit on the Ge concentration.²²

It remains to determine from the diffraction peak profiles the ratio of densities of two types of dislocations, and the correlation parameters for each type of dislocations.

TABLE I. In-plane strains in the layers ϵ , mean distances between dislocations $l = \rho^{-1}$, and the correlation parameters g obtained in the fits of reciprocal space maps for two samples 1 and 2.

	Layer composition	Layer thickness, nm	ϵ , %	90° dislocations		60° dislocations	
				$l = \rho^{-1}$, nm	g	$l = \rho^{-1}$, nm	g
Sample 1	Si _{0.14} Ge _{0.86}	1600	0.20	1299 ± 1100	0.96 ± 0.01	36 ± 2	0.99 ± 0.04
	Ge	1000	0.14	9.26 ± 0.03	0.32 ± 0.01
Sample 2	Si _{0.14} Ge _{0.86}	900	0.22	~3000	...	323	0.39
	Si _{0.17} Ge _{0.83}	100	0.28	146	0.36
	Si _{0.12} Ge _{0.88}	200	0.16	132	0.39
	Si _{0.08} Ge _{0.92}	200	0.15	115	0.40
	Si _{0.05} Ge _{0.95}	200	0.17	89	0.42
	Ge	1000	0.17	9.28 ± 3.87	0.13 ± 0.03	454	1.00 ± 0.30

The longitudinal and the transverse scans in symmetric and asymmetric reflections of a given layer, i.e., four independent measurements, can be used to obtain these three parameters. A good agreement between calculated and experimentally measured curves proves that the model is adequate. We use the longitudinal and transverse scans through the diffraction peaks to make the initial fits, since calculation of the whole RSM is a time-consuming procedure. Further refinement of the parameters is made by fitting the whole RSMs.

The parameters are fitted by using a nonlinear least-square fitting procedure (one of the versions of Levenberg-Marquadt algorithm²³). The error intervals for the parameters presented in Table I below are the root-mean-squared deviations of the parameters determined in the fits.

B. Two-layer Si_{1-x}Ge_x/Ge/Si epitaxial film

Figure 3 presents, by the color intensity distribution, the experimental reciprocal space maps of sample 1 in symmetric (004) and asymmetric ($\bar{2}24$) reflections. The sample contains a Ge buffer layer on the Si substrate and one Si_{1-x}Ge_x layer grown on the buffer. We find $x = 0.858$ from the diffraction peak positions. We refer to this layer as SiGe layer. The peaks in the asymmetric reflection follow the direction of the diffraction vector. However, both peaks are rigidly shifted

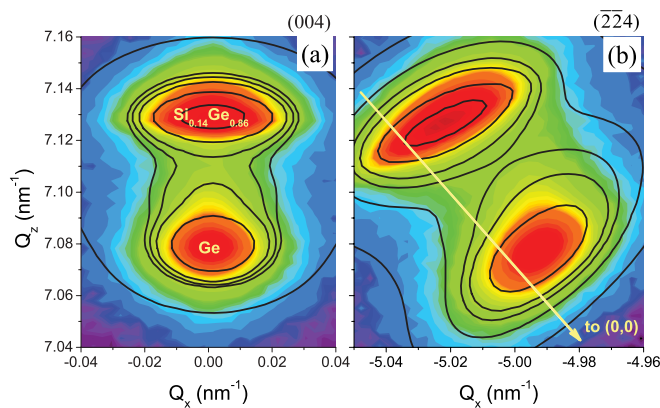


FIG. 3. (Color online) The reciprocal space maps of symmetric (004) and asymmetric ($\bar{2}24$) reflections of sample 1. The color intensity distribution are the experimental data, the contour lines present the calculated intensity distribution. The yellow arrow marks the direction from Si($\bar{2}24$) reflection to the origin of the reciprocal lattice.

from the relaxation line evidencing that both layers are slightly over-relaxed. This indicates the presence of extra tensile strain in the layers due to the different thermal expansion coefficients of substrate and layer materials.¹⁹ By means of equation (15) we obtained the strains to be equal to $\epsilon_{\text{SiGe}} = 0.20\%$ and $\epsilon_{\text{Ge}} = 0.14\%$ for the SiGe layer and Ge buffer, respectively. The peaks of both layers have elliptic shape, with different aspect ratios. In both reflections, the SiGe layer peak is notably more extended in the direction perpendicular to the diffraction vector. This difference points to different types of dislocations at the two heterointerfaces: the 60° dislocations give rise to larger aspect ratios than edge dislocations.¹⁰ The fit results presented below confirm this conclusion.

The calculated RSMs are shown in Fig. 3 as contour lines. The longitudinal and transverse scans through the SiGe and Ge peaks are compared in Fig. 4. Parameters obtained in the fit and used in the calculations presented above are listed in Table I. We find that only 90° dislocations are present at the substrate-buffer interface. The 60° dislocations were allowed in the fit, but their density has been found to be zero. The 90° dislocations are notably positionally correlated, giving the correlation parameter $g = 0.32$. The 60° dislocations dominate at the SiGe/Ge interface. They are uncorrelated, $g = 0.99$. This is also expected, since these dislocations glide in the inclined planes and are immobile after they reach the interface.

These results are in agreement with what observed in similar samples by Capellini *et al.*³ Using a very simple model and the results of plan view and cross sectional transmission electron microscopy (TEM) measurements, these authors have found that the strain in the Ge layer is released by the formation of highly ordered, [110] oriented 90° misfit dislocations at the Ge/Si interface directions, having an average distance of 9 nm, while the strain in the SiGe layer is released mostly by 60° dislocations, with misfit segments in the interface layer arranged in almost uncorrelated manner.

The peaks of the Ge buffer layer, both in symmetric and asymmetric reflections, have low-intensity tail in the direction to the SiGe peak. This tail extends mostly in the growth direction and is compatible with the presence of an alloyed transition layer at the interface. Supported by secondary ion mass spectroscopy results²⁰ we have included in the calculations a 100-nm-thick transition layer at the SiGe/Ge interface. This layer consisted of three compositional steps with same thicknesses and Ge content changing from the

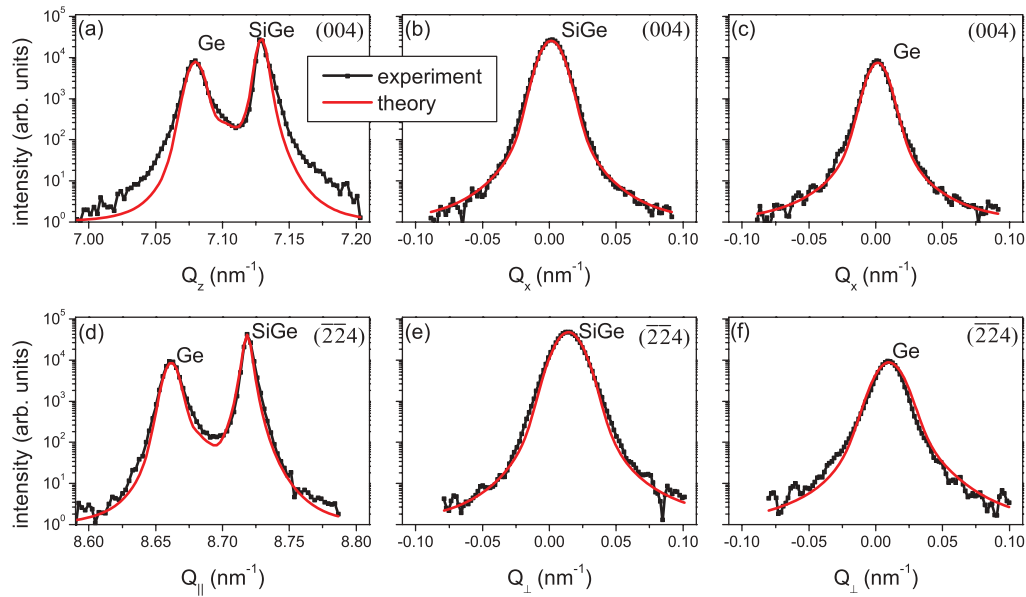


FIG. 4. (Color online) The longitudinal and transverse scans through the Ge buffer and SiGe top layer peaks of the sample 1.

bottom to the top as follows: $x = 0.987, 0.974, 0.962$. For the sake of simplicity, no dislocations were allowed between steps, as well as at the bottom interface. The addition of the transition layer improved the agreement between measured and simulated XRD data.

C. Many-layer SiGe/Ge/Si epitaxial film

The deposition procedure for sample 2 was programed in such a way to obtain a stack consisting of five $\text{Si}_{1-x}\text{Ge}_x$ layers on a Ge buffer layer. The experimental and calculated RSMs for this sample are presented in Fig. 5 both for (004) and $(\bar{2}24)$ reflections. The longitudinal and the transverse scans through diffraction peaks are shown in Fig. 6. Each peak in the RS scans displayed in Figs. 6(a) and 6(d) is associated to a layer in the sample stack.

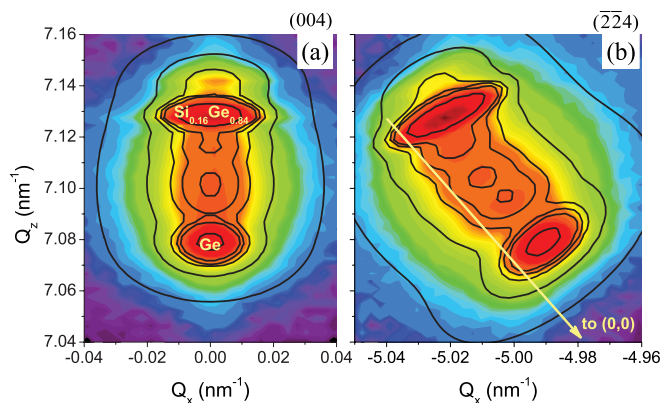


FIG. 5. (Color online) The reciprocal space maps of symmetric (004) and asymmetric $(\bar{2}24)$ reflections of sample 2. The color intensity distribution are the experimental data, the contour lines present the calculated intensity distribution. The yellow arrow marks the direction from $\text{Si}(\bar{2}24)$ reflection to the origin of the reciprocal lattice.

The analysis of the RSMs and the scans has been performed similarly to that for sample 1 in the previous section. The measured strain for each layer of the stack are reported in Table I. The reason for nonzero strain values was discussed in the previous section. The diffraction peaks of the Ge buffer and the top SiGe layer are well distinguished and allow the determination of the both types of dislocations. Thin intermediate layers have small dislocation densities and show only weak contrast at RSMs. These layers show distinct peaks in the asymmetric reflection but not in the symmetric one, see Figs. 5, 6(a), and 6(d). When both dislocation types are allowed in the calculation, the fit delivers comparable densities of two dislocation types with highly correlated 90° dislocations. This is unlikely, and we restrict the fit allowing only 60° dislocations at the intermediate interfaces.

The fit results are collected in Table I. For SiGe layers of sample 2, due to low dislocation densities or possible existence of (thin) transitional layers, the statistical errors are comparable with the corresponding parameter values. In this case, the estimated errors are not presented in the final results.

As in sample 1, the large misfit between Si substrate and Ge buffer layer is plastically relaxed by means of 90° dislocations. The dislocation densities in samples 1 and 2 almost coincide, since the misfit between Si and Ge is completely relaxed in both cases. However, in sample 2, the dislocations at Ge/Si interface are much better correlated, with approximately three times smaller correlation parameter g . The difference between samples is clearly visible by comparing the widths of the Ge peaks in RSMs in Figs. 3 and 5: the Ge peaks of sample 2 are notably sharper, given the same dislocation density.

The growth procedure and the overall thermal budget of the two investigated samples is nominally identical, and thus the misfit dislocations should have had the same “drive” to correlate. We believe that the different degree of correlation observed here can be due to experimental parameter fluctuations during the initial low-temperature deposition step of the relaxed Ge layer. As a matter of fact, owing to the closeness

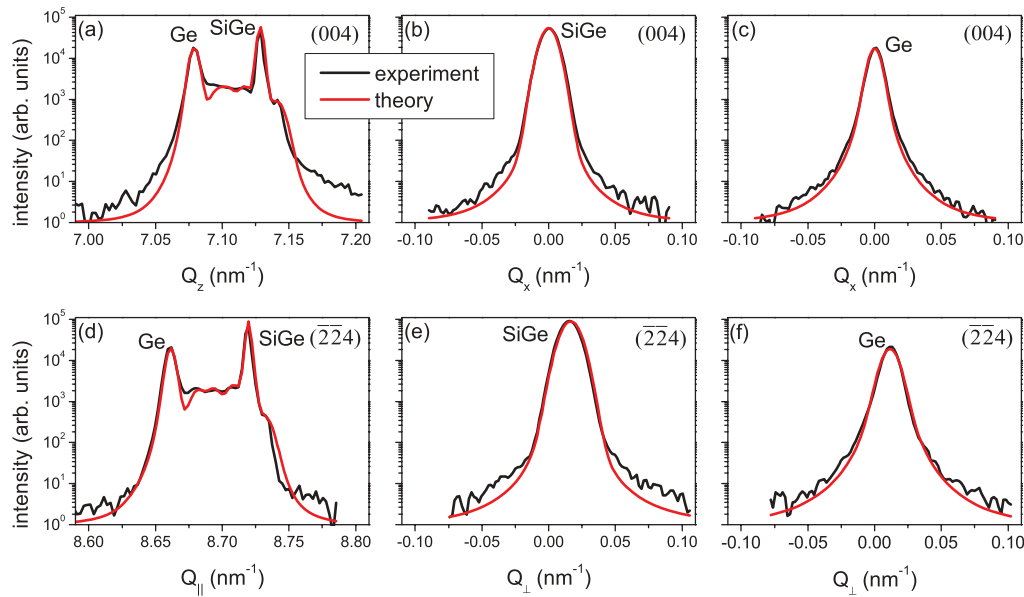


FIG. 6. (Color online) The longitudinal and transverse scans through the Ge buffer and SiGe top layer peaks of the sample 2.

of the deposition temperature (~ 330 °C) to the dihydride desorption temperature (~ 350 °C) from Ge/Si surfaces,²⁴ slight changes in the growth temperature or in its reading can drive major changes to the ad-molecules mobility and, consequently, to the structural quality of the heterointerface. This can have an impact on the nucleation of the misfit dislocations and on their mobility at the early stage of the growth, thus leading to a different spatial correlation.

Both types of dislocations are also allowed in the fit of the top SiGe layer, but the fit results in Table I show that mostly 60° dislocations are present at the top interface. These dislocations are correlated ($g = 0.39$), in contrast to sample 1 where 60° dislocation at the SiGe/Ge interface are completely uncorrelated. We believe that this enhanced correlation can be due to the lower density of MDs injected at each interface of sample 2 compared to the higher strain relaxation occurring at the single heterointerface of the RGVS present in sample 1.

V. CONCLUSIONS

Misfit dislocations in the SiGe/Ge/Si multilayer epitaxial system have been studied by x-ray diffraction. Kinematical calculation of the x-ray intensity is made for different dislocation types, densities, correlations at different interfaces. Good agreement between fit results and the experiment allows to describe the dislocation network. The fits show that the Ge/Si interface contains highly positionally correlated edge dislocations, while the SiGe/Ge interface contains uncorrelated/little correlated 60° dislocations.

ACKNOWLEDGMENTS

The work has been partially funded by Deutsche Forschungsgemeinschaft (DFG) grant KA 3262/2-1. GC is grateful for the “IHP International Fellowship Award 2011.”

*victor.kopp@pdi-berlin.de

¹See *International Technology Roadmap for Semiconductors*, <http://www.itrs.net>.

²D. Paul, *Laser Photon. Rev.* **4**, 610 (2010).

³G. Capellini, M. D. Seta, Y. Busby, M. Pea, F. Evangelisti, G. Nicotra, C. Spinella, M. Nardone, and C. Ferrari, *J. Appl. Phys.* **107**, 063504 (2010).

⁴V. A. Shah, A. Dobbie, M. Myronov, and D. R. Leadley, *J. Appl. Phys.* **107**, 064304 (2010).

⁵R. Hull and J. C. Bean, *Crit. Rev. Solid State* **17**, 507 (1992).

⁶S. C. Jain, A. H. Harker, and R. A. Cowley, *Philos. Mag. A* **75**, 1461 (1997).

⁷Y. B. Bolkhovityanov, O. P. Pchelyakov, and S. I. Chikichev, *Phys. Usp.* **44**, 655 (2001).

⁸U. Pietsch, V. Holý, and T. Baumbach, *High-Resolution X-Ray Scattering: From Thin Films to Lateral Nanostructures* (Springer, Berlin, 2004).

⁹M. A. Krivoglaz, *X-Ray and Neutron Diffraction in Nonideal Crystals* (Springer, Berlin, 1996).

¹⁰V. M. Kaganer, R. Köhler, M. Schmidbauer, R. Opitz, and B. Jenichen, *Phys. Rev. B* **55**, 1793 (1997).

¹¹V. M. Kaganer and K. K. Sabelfeld, *Phys. Rev. B* **80**, 184105 (2009).

¹²V. M. Kaganer and K. K. Sabelfeld, *Phys. Status Solidi A* **208**, 2563 (2011).

¹³V. Holý, J. H. Li, G. Bauer, F. Schäffler, and H.-J. Herzog, *J. Appl. Phys.* **78**, 5013 (1995).

¹⁴J. H. Li, V. Holý, G. Bauer, and F. Schaffler, *J. Appl. Phys.* **82**, 2881 (1997).

- ¹⁵S. Danis, V. Holý, J. Stangl, and G. Bauer, *Europhys. Lett.* **82**, 66004 (2008).
- ¹⁶A. Benediktovitch, A. Ulyanekov, F. Rinaldi, K. Saito, and V. M. Kaganer, *Phys. Rev. B* **84**, 035302 (2011).
- ¹⁷A. Zhylik, A. Benediktovich, A. Ulyanekov, H. Guerault, M. Myronov, A. Dobbie, D. R. Leadley, and T. Ulyanekova, *J. Appl. Phys.* **109**, 123714 (2011).
- ¹⁸L. Colace, G. Masini, F. Galluzzi, G. Assanto, G. Capellini, D. Gaspare, E. L. Palange, and F. Evangelisti, *Appl. Phys. Lett.* **72**, 3175 (1998).
- ¹⁹G. Capellini, M. De Seta, P. Zaumseil, G. Kozlowski, and T. Schroeder, *J. Appl. Phys.* **111**, 073518 (2012).
- ²⁰M. De Seta, G. Capellini, M. Ortolani, M. Virgilio, S. Lupi, G. Grosso, G. Pizzi, P. Zaumseil, and G. Nicotra (unpublished).
- ²¹Y. Epelboin, M. Gandais, and C. Willaime, *Phys. Status Solidi A* **44**, 651 (1977).
- ²²J. P. Dismukes, L. Ekstrom, and R. J. Paff, *J. Phys. Chem-US* **68**, 3021 (1964).
- ²³M. Lourakis, *Levmar: Levenberg-Marquardt Nonlinear Least Squares Algorithms in C/C++* (2004), <http://www.ics.forth.gr/~lourakis/levmar/index.html>.
- ²⁴T. Angot and P. Louis, *Phys. Rev. B* **60**, 5938 (1999).